Post-synthetic ligand exchange as a route to improve the affinity of ZIF-67 towards CO_2

David Villalgordo-Hernández [a], Manuel Antonio Diaz-Perez [b], Valentina Balloi [b],
Mayra Anabel Lara-Angulo [b], Javier Narciso [a], Juan Carlos Serrano-Ruiz [b],
Enrique V. Ramos-Fernandez [a,*]

[a] *Laboratory of Advanced Materials, Inorganic Chemistry Department, University Materials Institute of Alicante, University of Alicante. Apartado 99, E-03080 Alicante, Spain*
[b] *Materials and Sustainability Group, Department of Engineering, Universidad Loyola Andalucía, Avenida de las Universidades, s/n, 41704 Sevilla, Spain*

A B S T R A C T

The Zeolitic Imidazolate Framework 67 (ZIF-67) is a highly promising material owing to its exceptional thermal stability, large specific surface area, cost-effectiveness, and versatile applications. One of the potential applications of ZIF-67 is gas separation processes, among which the separation of CO_2/CH_4 mixtures has attracted great interest nowadays in the biogas sector. However, when it comes to CO_2/CH_4 separation, ZIF-67 falls short as it lacks the desired selectivity despite its high adsorption capacity. This limitation arises from its relatively low affinity towards CO_2. In this study, we have addressed this issue by partially exchanging the ligand of ZIF-67, specifically replacing 2-methylimidazole with 1,2,4 (1H) triazole, which introduces an additional nitrogen atom. This modification resulted in ZIF-67 showing significantly enhanced affinity towards CO_2 and, as a result, greater selectivity towards CO_2 over CH_4. The modified materials underwent thorough characterization using various techniques, and their adsorption capacity was evaluated through high-pressure adsorption isotherms. Furthermore, their separation performance was assessed using the Ideal Solution Adsorption Theory, which provided valuable insights into their potential for efficient gas separation.

1. Introduction

The separation of CH_4 and CO_2 is a topic of great interest, especially for the recovery of methane from biogas and natural gas. In both processes, methane is often contaminated with CO_2, which needs to be removed. This purification step is essential to allow the methane to be transported through the gas distribution network, as it helps avoid corrosion. In addition, separation allows the calorific value of the gas mixture to be increased, making it more valuable for various applications [1–7].

The separation of CH_4 and CO_2 has been widely studied and various methods have been implemented, with amine absorption being the most advanced commercial technology at present. However, cryogenic distillation and membrane processes have also received growing attention [8–13]. While amine adsorption and cryogenic distillation are energy-intensive technologies, membrane separation is less costly in terms of energy although it still suffers from lack of selectivity and stable membranes [3,14–16].

Adsorption technologies such as pressure swing adsorption (PSA) and temperature swing adsorption (TSA) have emerged as viable options for CH_4 purification from natural gas or biogas. These methods have shown great potential and offer opportunities to expand CH_4 utilisation. The choice of adsorbent is key for developing PSA and TSA technologies. Adsorbents are required to have high capacity, easy regeneration, long life and, above all, a high selectivity towards CO_2 during the adsorption process. This selectivity towards CO_2 is required to be high at low pressures if they are to be used for biogas purification, while high selectivity at high pressures is more relevant for natural gas recovery. [17,18]. The most commonly used porous materials for this application are zeolites and activated carbons since they are highly stable, cheap and well-known.

Metal-organic frameworks (MOFs) have attracted great interest in recent years due to their versatility and potential applications in storage, separation, catalysis and gas sensing [19–26]. Among the hundreds of thousands of MOFs developed in recent years, ZIF-67 (zeolitic imidazolate framework-67) stands out for its exceptional stability and high surface area. However, the exploration of strategies to chemically modify ZIF-67 while preserving its topology has become a topic of considerable research interest [27,28].

MOFs have emerged as a potential material for the separation of CH_4/CO_2 mixtures. However, many of them are unstable and suffer for degradation upon use. ZIFs materials, especially ZIF-67, have been

---

shown to combine high stability and high specific surface area, although this material suffer from low affinity towards CO_2 [1,29,30]. Several strategies have been devised to enhance the CO_2 affinity of ZIF-67. Some involve encapsulating molecules with a high CO_2 affinity (e.g., ionic liquids) within its structure, while others focus on modifying the surface chemistry of ZIF-67 to introduce functional groups with CO_2 affinity [31–34]. This can be achieved either by incorporating a second metal in the structure to create defects that enhance CO_2 affinity or by adding a linker capable of strong CO_2 adsorption to the network. In this article, we will focus on the latter approach and present a method for incorporating nitrogen functionalities that serve as anchoring centers for CO_2 [35,36]. Thus, modification with an appropriate ligand (triazole-type) to improve the affinity for CO_2 is essential. The tailored chemical environment and pore characteristics of the triazole-modified ZIF-67 are expected to impart improved adsorption selectivity, enabling efficient separation of these two gases at different conditions [27,29,30,37,38].

In this study, we present a ligand exchange-mediated modification approach to enhance the chemical properties of ZIF-67 without compromising its topological integrity. Specifically, we focus on replacing a fraction of the original 2-methylimidazole ligands in ZIF-67 with triazole molecules 1,2,4(1H)triazole (Trz). This ligand exchange strategy enables us to introduce new chemical functionalities into the framework, thereby tailoring its reactivity and adsorption properties. Furthermore, we evaluated the performance of the modified ZIF-67 as a promising material for the separation of methane and carbon dioxide.

2. Experimental

2.1. MOF synthesis and characterization

The experimental details are provided in the supporting information.

3. Results and discussion

The aim of this research paper is to increase the CO2 affinity of ZIF-67 by partially substituting the current ligands (2-methylimidazole) in ZIF-67 with a triazole-type ligand (1,2,4-1H-triazole) using a post-synthetic approach. This substitution is intended to prevent one of the nitrogen atoms in the triazole group from coordinating with the metal. By leaving this nitrogen uncoordinated, it can function as a basic center, thereby enhancing the CO2 affinity. Before proceeding with the replacement of 2-methylimidazole with 1,2,4-1H-triazole, we optimized the ZIF-67 synthesis to achieve crystals with a narrow size distribution, high specific surface area, and an optimal truncated dodecahedral rhombic crystal morphology [12–14]. This optimized synthesis of ZIF-67 is summarized in the supplementary information (Table S1). The optimized ZIF-67 sample (sample 7) showed a specific surface area of 1359 m^2/g, which falls within the typical range reported in the literature for this kind of materials [29,30,38]. Furthermore, the crystals display a truncated dodecahedral rhombic morphology (Figure S5).

The exchange was performed by mixing a methanolic suspension of ZIF-67 with a solution of triazole in methanol. The resulting mixture is then stirred for a duration of 3 days. Afterwards, the MOF is separated through centrifugation and subjected to 10 washes using methanol. This process is carried out to remove any ligands that are not firmly attached to the structure. Different concentrations of triazole were utilized in the exchange process with the intended goal of replacing 10 % (ZIF-67 m0.2), 50 % (ZIF-67 m0.5), 100 % (ZIF-67 m1.1) of the 2-methylimidazole present in ZIF-67. Additionally, an excess of triazole (200 % concentration, ZIF-67 m1.2) was also used, as detailed in the experimental section. Furthermore, a sample (Co-Trz) was prepared in which triazole was directly mixed with the metal precursor to assess the formation of a ZIF-67 analogue using triazole following the same procedure employed for the optimized ZIF-67 sample (sample 7, supporting information).

Fig. 1 illustrates the diffraction patterns of the samples subjected to different percentages of triazole exchange, as well as the sample directly
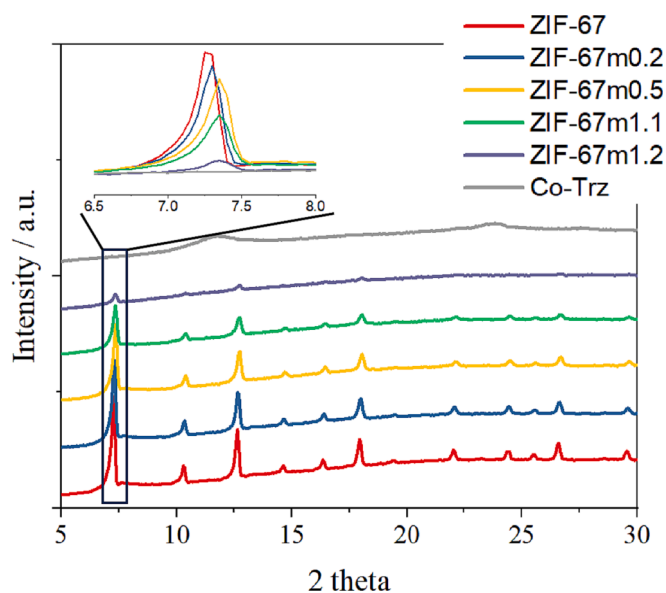

Fig. 1. Diffraction patterns of ZIF-67 and samples exchanged with different proportions of triazole, along with the sample prepared directly with triazole. The inset highlights the shift of the main peak towards higher 2 theta values.

synthesized with triazole. Notably, the sample synthesized directly with triazole exhibits no discernible diffraction peaks, suggesting that the direct synthesis of a ZIF-67 analogue with triazole is not possible at the used synthesis conditions. On the other hand, all the exchanged samples showed a diffraction pattern consistent with that of ZIF-67, indicating that the exchange process has not altered the fundamental structure of ZIF-67, even at high nominal exchange rates.

Analyzing the most prominent peak, centered at $2\theta = 7.3$, we observe a slight shift towards higher angles as the nominal exchange rate increases. This shift signifies a reduction in the d-spacing, implying that the structure underwent contraction as the degree of exchange increased.

Field-emission scanning electron microscopy (FE-SEM, Fig. 2) clearly demonstrate that the crystals maintain their original morphology and size even after undergoing the exchange treatment. This observation, coupled with the XRD results, provides compelling evidence that the crystal structure and morphology remain unchanged throughout the exchange process. The sample directly synthesized with triazole exhibits a distinct morphology (needle-shaped crystals, not shown) that differs significantly from the typical ZIF-67 crystals. Notably, even when achieving a relatively high exchange degree of ZIF-67 m1.2, the crystals retain the same morphology as the unexchanged ZIF-67. This finding emphasizes the robustness of the crystal morphology throughout the exchange process, indicating that the underlying structure of ZIF-67 remains intact despite significant ligand substitution.

In order to determine the precise degree of ligand exchange it is necessary to perform a quantitative analysis on the solid material. However, this analysis is challenging since both 2-methylimidazole and triazole ligands are integral components of the MOF structure. Traditional techniques such as infrared spectroscopy (FTIR), XRD, or X-ray photoelectron spectroscopy (XPS) are not suitable for quantitative analysis. To address this, we developed a method involving the dissolution of the materials in deuterated sulfuric acid (D_2SO_4). The resulting solution is then subjected to analysis using nuclear magnetic resonance (^1H NMR), allowing us to calculate the ratio of triazole to 2-methylimidazole. As shown in Table 1, the nominal exchange was not achieved for any of the samples. For instance, ZIF-67 m0.2, intended to reach 20 % exchange, only achieved 6.6 % exchange. Similar trends were observed for all the samples [39].

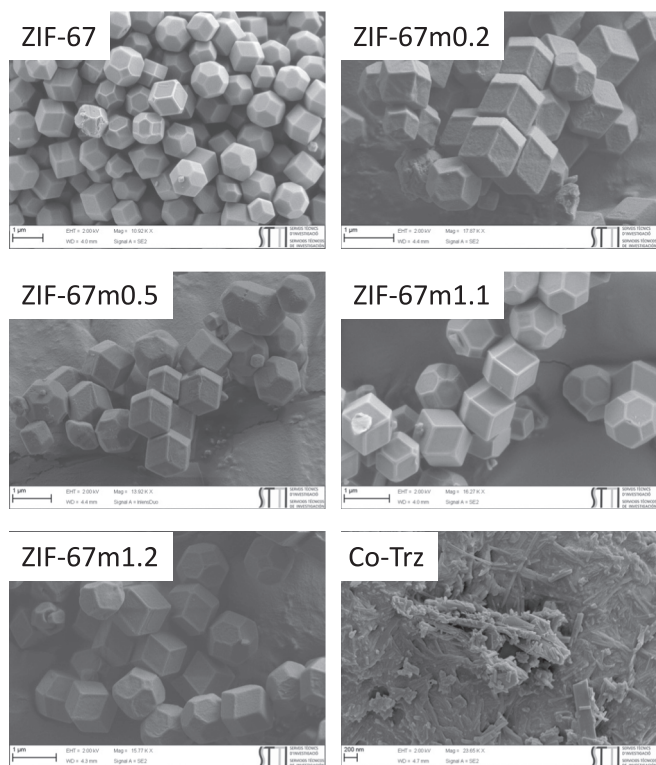The TG profile of the ZIF-67 synthetized herein (Fig. 3) revealed a

Fig. 2. SEM images of ZIF-67 and samples with varying proportions of triazole exchange, including the sample directly prepared using triazole and the unmodified one.

Table 1
Characterisation of the porous texture of the different materials obtained from nitrogen adsorption isotherms. The actual degree of ligand exchange was determined by ^1H NMR.

Sample	% of linker exchanged calculated by ^1H NMR	$S_{B.E.T.}$ m^2/g	V_{micro} cm^3/g
ZIF-67	–	1359	0.8
ZIF-67 m0.2	6.6	1251	0.71
ZIF-67 m0.5	11.2	1020	0.58
ZIF-67 m1.1	27.9	701	0.38
ZIF-67 m1.2	66.9	174	0.09

single mass drop above 600 °C, in line with the expected thermal behaviour of this sample [1]. Remarkably, the Co-Trz sample showed a distinct profile, featuring multiple mass drops, with the most prominent one observed at 420 °C. The exchanged samples showed lower thermal stability as compared to ZIF-67, with two mass losses at temperatures below 600 °C. Furthermore, the absence of mass losses occurring at the same temperature as ZIF-67 suggests that all the crystals have been uniformly exchanged. Otherwise, some of the mass losses would coincide with the temperature ranges corresponding to unmodified ZIF-67 crystals, particularly noticeable in samples with a low degree of exchange.

Literature indicates that zinc triazolates are generally less stable than Zn imidazolates [28]. Therefore, these thermographic curves corroborate the presence of triazole in the crystals, which contributes to their lower stability. Furthermore, a correlation between the degree of exchange and the stability of the samples can be inferred from the data. The correlation becomes evident when we create a graph that plots the temperature at which the material loses half of its mass against the
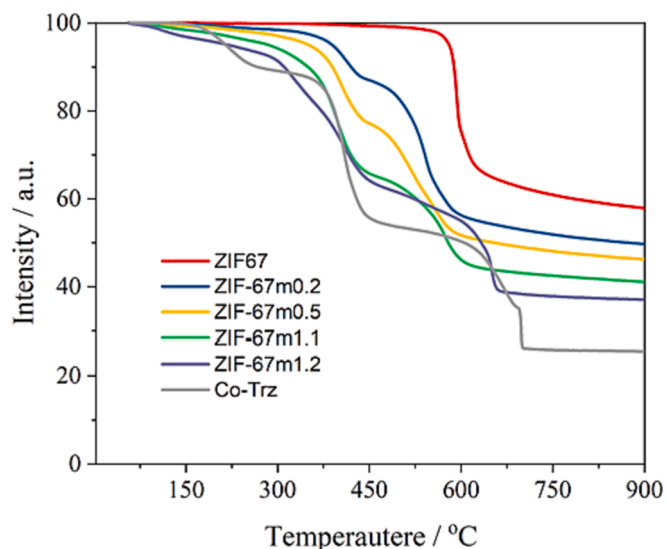

Fig. 3. TGA profiles of ZIF-67 and samples undergoing varying triazole exchange, along with the sample directly prepared using triazole.

degree of exchange. You can find this graph in the supporting information for reference (Fig s.

By analyzing the gases emitted during the thermograms, we can identify the specific fragments released at different temperatures. This allows us to determine whether the two mass drops observed in the samples correspond to the exchanged portion and the pure ZIF-67 phase, thereby revealing the presence of segregated phases Fig. 4.

For the 2-methylimidazole analysis, we have monitored the fragments with mass/charge ratios (m/z) of 82 and 54. Similarly, in the case of 1,2,4-1H-triazole, we tracked the fragment with m/z values of 69. Additionally, we have monitored the fragment with an m/z value of 44 to resonance stabilized nitrogen containing cations. These specific fragments serve as indicators to differentiate the volatilised linkers their respective decomposition products Fig. 4.

The profiles of the ZIF-67 samples show a prominent peak for m/z values of 42, 54 and 82 signal at ca. 600 °C, revealing the decomposition of ZIF-67 and the release of the linker. Furthermore, this signal is accompanied by the m/z 44 signal, indicating that the decomposition of the ligand generated nitrogen compounds. In contrast, the sample synthetized directly with triazole shows a different decomposition pattern, with two emission peaks at m/z 69 and 42. The first peak at 260 °C, which is the boiling point of triazole, suggesting that part of the ligand is not coordinated to the metal. The second main peak at 400 °C was ascribed to the decomposition of the structure. The exchanged sample ZIF-67 m1.2 showed a significantly different decomposition profile. Signals corresponding to 2-methylimidazole (m/z 82) and triazole (m/z 69) were observed within the 300–400 °C temperature range, suggesting that the gases coming for both ligands were released simultaneously during this process. It should be noted that the triazole signals showed a secondary deconvolution at a slightly higher temperature (420 °C), possibly due to the fact that the decomposition of the triazole occurs in two distinct stages. These results confirm that the exchange is uniform and produces a change in the stability of the material, as expected.

The obtained results collectively demonstrate that our synthetic method enables the exchange of a portion of 2-methylimidazole, a constituent of ZIF-67, while maintaining its structural integrity. Based on these findings, our subsequent efforts concentrated on thoroughly characterizing the textural and chemical attributes of the exchanged materials.

Fig. 5A illustrates the nitrogen adsorption isotherms of the samples under study. The Co-Trz sample showed a significantly low adsorption capacity at low relative pressures (50 cm^3 (STP)/g), with gradual uptake

ZIF-67

Co-Trz
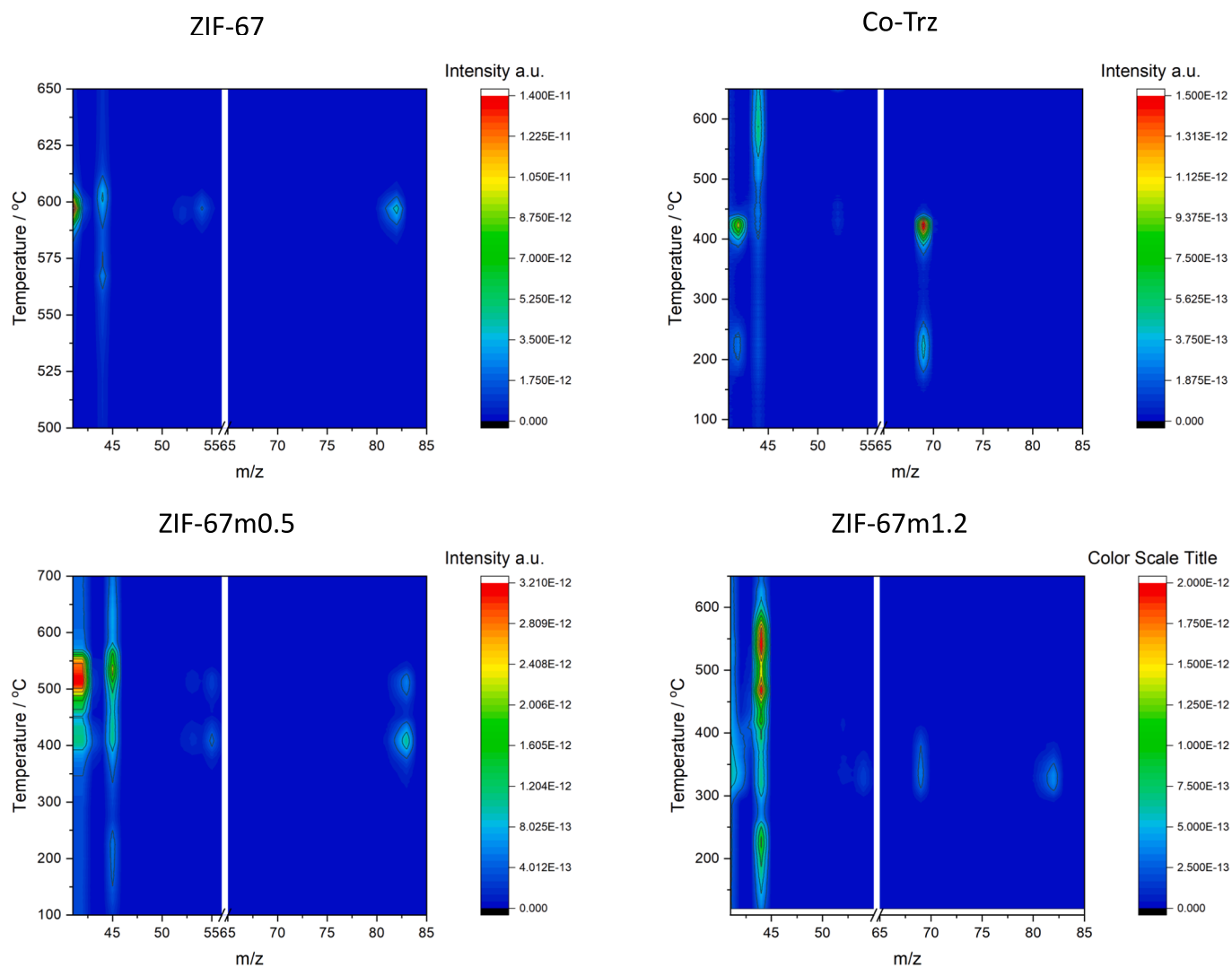

ZIF-67m0.5

ZIF-67m1.2

Fig. 4. Depicts the mass signal profiles emitted during the thermograms. three samples are illustrated: zif-67, the sample prepared directly with triazole, and two exchanged samples (zif-67 m0.5 and ZIF-67 m1.2).
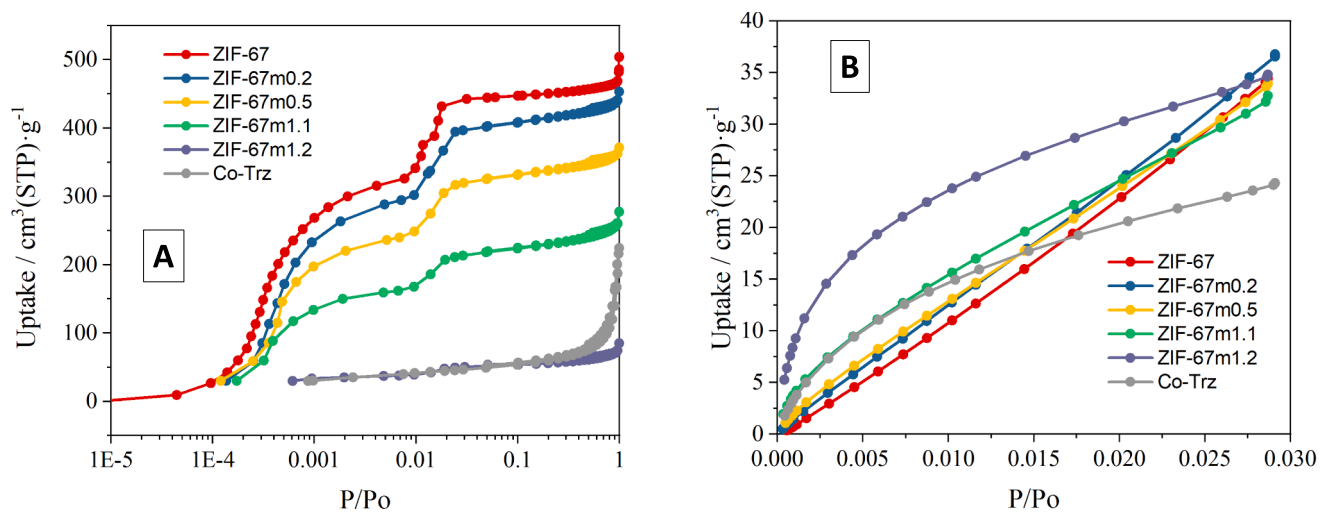

Fig. 5. N$_2$ adsorption isotherms at 77 K (A) and the CO$_2$ adsorption isotherms at 273 K (B) for the ZIF-67 the exchanged samples and the sample prepared with triazole.

increase starting from 0.2 relative pressure, indicating the presence of a small portion of mesopores. On the other hand, both ZIF-67 and the exchanged samples showed a typical type I isotherm characteristic of microporous ZIF-type materials. Furthermore, they display two steps at low relative pressures, which is indicative of the structural flexibility observed for this material, in line with other works, including reports from our group [40,41]. The N_2 adsorption isotherms is plotted in logarithmic scale to better distinguish these two stages. There is a clear correlation between the adsorption capacity and the degree of exchange: the higher the exchange, the lower the adsorption capacity. This decrease in adsorption capacity is due to the shrinkage of the structure, as revealed by XRD (Fig. 1).

The observed structural shrinkage, combined with the likely presence of unconnected nitrogen, suggests a higher affinity for CO_2. To investigate this, CO_2 adsorption isotherms were conducted at 273 K to assess the affinity of the solids towards CO_2 (Fig. 5B). The linear CO_2 isotherm of pure ZIF-67 revealed low affinity towards CO_2. In contrast to ZIF-67, materials with a high degree of exchange exhibited a curved isotherm, demonstrating rapid CO_2 adsorption at low pressures. Notably, despite having significantly lower surface area than ZIF-67, the exchanged samples consistently showed higher CO_2 adsorption capacities at low pressures. This suggests that either the structural shrinkage (resulting in pore narrowing) or the presence of uncoordinated nitrogen contributes to an increased affinity for CO_2.

We conducted FTIR and Raman spectroscopy with the aim to identify the functional groups present in the exchanged materials (Figures S4 y S5). As the degree of exchange increases, multiple peaks become apparent in the infrared spectrum. These peaks can be attributed to the presence of coordinated triazole within the structure. Both techniques revealed bands corresponding to nitrogen atoms not coordinated to the metal (686 cm^{-1} and 1290 cm^{-1} for the FTIR and Raman spectra, respectively) [42–45]. This finding is significant since it provides evidence supporting the higher affinity for CO_2 exhibited by the exchanged samples.

XPS provides valuable insights into the electronic properties of the various samples. Fig. 6 show the N 1 s level, revealing noticeable differences among the samples. Specifically, ZIF-67 exhibits a peak centered at 398.8 eV, which can be attributed to nitrogen being part of the ZIF-67 structure. However, for the exchanged samples, the N 1 s band shifted to higher binding energies and showed a shoulder, allowing us to deconvolute the signal into two distinct contributions: one at 399 eV and another at a higher binding energy. The peak at higher binding energies, particularly noticeable for the Co-Trz sample, has been previously ascribed to doubly bonded nitrogen atom (-N = N-) from the triazole units of the network [43,46]. These findings suggest that the incorporation of triazole into the structure is taking place. As the degree of exchange increases, the intensity of the peak at higher binding energies also increases. This observation aligns with and provides further confirmation of the earlier results.

Upon examining the Co 2p spectra (Fig. 6b), notable differences can be observed among the various samples. For instance, in the ZIF-67 sample, two broad peaks appear at 781 eV (Co $2p_{3/2}$) and 796 eV (Co $2p_{1/2}$), corresponding to Co(II) species. This identification is further supported by the presence of satellite peaks between 784 and 790 eV. This spectrum aligns with the published data for this material [29,30,37,47]. When shifting the focus to the Co-Trz sample and analyzing its spectrum, a peak at 782 eV (Co $2p3/2$) and another at 797.01 eV (Co $2p1/2$) become apparent, with the satellite peaks being indiscernible. Upon reviewing the literature, it is found that this peak can be attributed to the presence of Co(III). This finding is highly
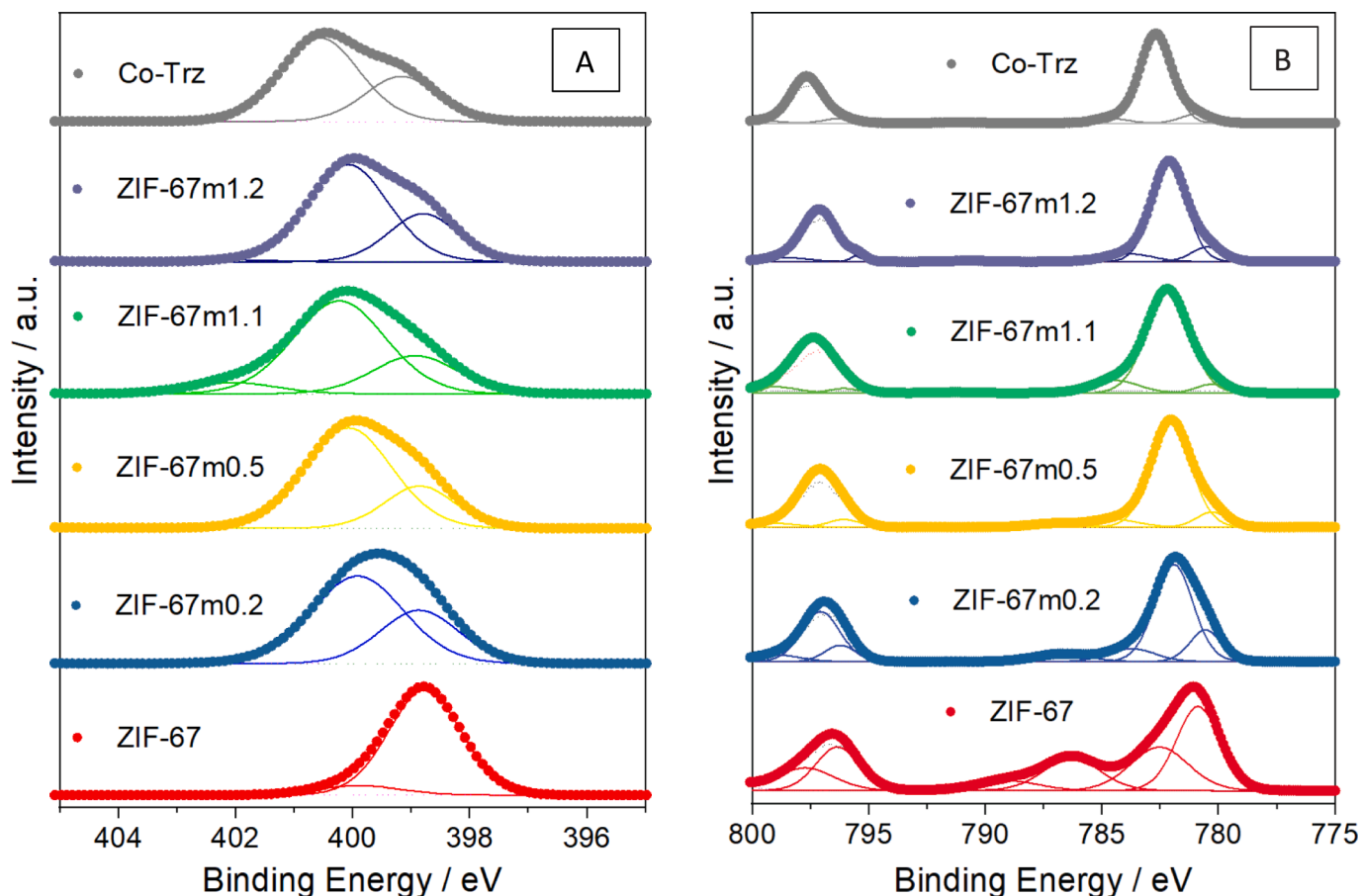

Fig. 6. Shows the results of x-ray photoelectron spectroscopy. a is the 1 s core level of N, B plot the2p core level of cobalt.

relevant as it indicates that during the synthesis of Co-Trz, the Co(II) species undergo oxidation to Co(III). The exchanged samples exhibit an intermediate behavior, and it can be observed that as the degree of exchange increases, the degree of Co oxidation also rises [48].

The change in cobalt's oxidation state is accompanied by a noticeable shift in the sample's colour. ZIF-67 exhibits an intense blue, almost violet, while Co-Trz displays an orange colour. This colour transformation was previously observed by Erkartal et al. [27] when exchanging ZIF-67 with a different triazole, although they did not conduct a spectroscopic study to determine the Co oxidation state. Nonetheless, their findings provide valuable insights into the phenomenon.

Erkartal et al. [27] discovered that the exchange process resulted in a shift in the coordination of Co from tetrahedral to octahedral. They found that all the nitrogens in the triazole coordinated with cobalt in their study. In our case, however, we observed that the nitrogens were not coordinated to cobalt, indicating that the octahedral coordination responsible for the color change might be the origin of the Co(III) oxidation state. Although the specific mechanisms behind this oxidation state change are not explored in this paper, we intend to investigate it in future research. We believe that understanding this process could open up new possibilities for preparing mixed valence MOFs [49].

Based on the obtained results, it is evident that it is feasible to achieve partial exchange of 2-methylimidazole with 1,2,4(1H)triazole while preserving the crystal structure and morphology of ZIF-67. With this successful demonstration, we proceeded to utilize three of these exchanged materials for separation of CH_4/CO_2 for the valorization of natural gas or biogas.

3.1. Methane carbon dioxide separation

To assess the adsorption capacity of the materials, CO_2 and CH_4 adsorption isotherms at high pressure were conducted on three samples representing the limiting cases and one intermediate sample (ZIF-67, ZIF-67 m1.1, ZIF-67 m1.2). The results are shown in Fig. 7. It can be observed that the CO_2 adsorption capacity is higher than that of CH_4 in all three samples. This indicates that all three materials should, in principle, exhibit equilibrium selectivity towards CO_2 adsorption. Another significant finding is that the adsorption capacity of the exchanged samples is lower compared to the original sample. This aligns with the characterization results, which revealed a contraction in the structure and a significant reduction in the specific surface area of the material. Upon closer examination of the CO_2 isotherms, it becomes evident that the curvature at pressures below 1000 kPa becomes more pronounced in the sample with higher exchange rates (ZIF-67 m1.2). This observation suggests a stronger affinity of the material for CO_2 compared to the other samples.

These results once again demonstrate that the surface chemistry of these materials can be modified through ligand exchange, resulting in materials with higher affinity towards CO_2 while maintaining the ZIF-67 base structure. To qualitatively assess this, we measured the adsorption isotherms at three different temperatures (see supporting information) and calculated the isosteric heats of adsorption (Figure S6).

It is interesting to observe that the ZIF-67 m1.1 and ZIF-67 m1.2 samples exhibit higher CO_2 adsorption heats at low coverage compared to the ZIF-67 sample. This suggests that the interaction between CO_2 and the exchanged samples is stronger, indicating a higher affinity. Furthermore, we note that the exchange process does not significantly affect the adsorption heats of CH_4, which remain nearly constant and lower than those of CO_2 across the entire coverage range for all three samples.

The selectivity of CO_2/CH_4 adsorption in binary mixtures can be determined using the Ideal Adsorption Solution Theory (IAST), a widely utilized approach for predicting gas separation in various porous materials such as porous carbon, zeolites, MOFs, and porous polymers [50,51]. The calculations for selectivity are described in detail in the
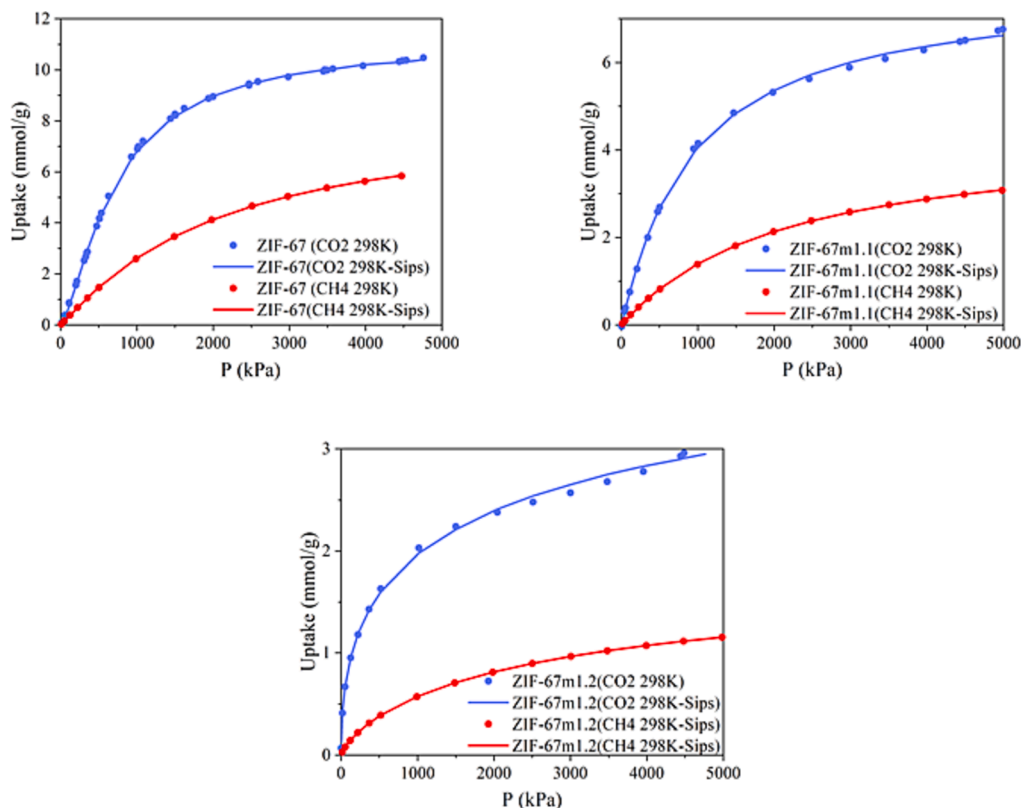

Fig. 7. Shows the high-pressure isotherms of ch₄ and CO2 for three different samples. The dots indicate the experimental data while the lines are the result of fitting the experimental data to the Sips isotherm model.

supporting information.

To begin, we employed the Sips isotherm model to fit the experimental data [52,53]. The fitted curves, displayed in Fig. 7, demonstrate excellent agreement with the experimental points, accurately representing the isotherm behavior. Once the model parameters were determined, the fitting function was utilized to calculate the CO_2/CH_4 selectivity for different compositions of CO_2/CH_4 mixtures (see supporting information to see calculation details as well as the Matlab code).

When examining the ZIF-67 sample, we observed a consistent selectivity ranging from 1.5 to 4 across the entire pressure range and for all CO_2 percentages in the mixture Fig. 8. These findings align with previously published data for ZIF-67 [2,14]. Moving on to the ZIF-67 m1.1 sample, we observe an increase in selectivity with both pressure and CO_2 concentration in the mixture [6]. Interestingly, for the ZIF-67 m1.2 sample, the selectivity reaches an outstanding value of above 30, which is notably high for this type of sample and application compared to the existing literature [2,4,6,14]. In the supporting information, we have included a table (table S2) that compares the selectivity values obtained in our study with those from other ZIF and modified ZIF materials. This additional information is provided for the benefit of the reader.

We attribute this enhancement to two underlying effects. Firstly, the contraction of the structure leads to a more pronounced sieving effect, as the kinetic diameter of CO_2 is 3.3 Å and CH_4 is 3.8 Å. This size difference allows for more selective adsorption of CO_2 over CH_4 within the material's pores.

Secondly, the presence of uncoordinated nitrogen sites, which exhibit affinity for CO_2 compared to CH_4. These nitrogen sites selectively interact with CO_2 molecules.

The combined influence of these effects, the enhanced sieving effect and the presence of uncoordinated nitrogen sites, synergistically contributes to the improved selectivity of the exchanged samples towards CO_2 over CH_4.

These results indicate that ZIF-67 has very poor properties for use as a molecular sieve for CO_2 and CH_4. However, when the material is modified, its separation capacity changes. Thus, when using the ZIF-67 m1.1 sample, the material separates CO_2 at high pressures better than at low pressures. This makes it ideal for high pressure applications such as the valorisation of CO_2 that is extracted from natural gas wells. While the ZIF-67 m1.2 sample is more selective at lower pressures, making it ideal for biogas purification.

4. Conclusions

This study reveals a finding regarding the exchange of a portion of the ligand within the ZIF-67 structure with a 1,2,4 1H-triazole ligand. This exchange leads to two crucial effects: structural contraction and the emergence of uncoordinated nitrogen sites. These combined effects result in the modified material exhibiting a higher affinity for CO_2 compared to CH_4, thereby significantly enhancing its selectivity for CO_2 adsorption over the original ZIF-67 material.

As a result, the exchanged material demonstrates improved CO_2 selectivity compared to the original ZIF-67 structure. This understanding provides valuable insights for tailoring materials with enhanced CO_2 capture capabilities and underscores the importance of structure engineering and chemical design in optimizing gas adsorption performance.
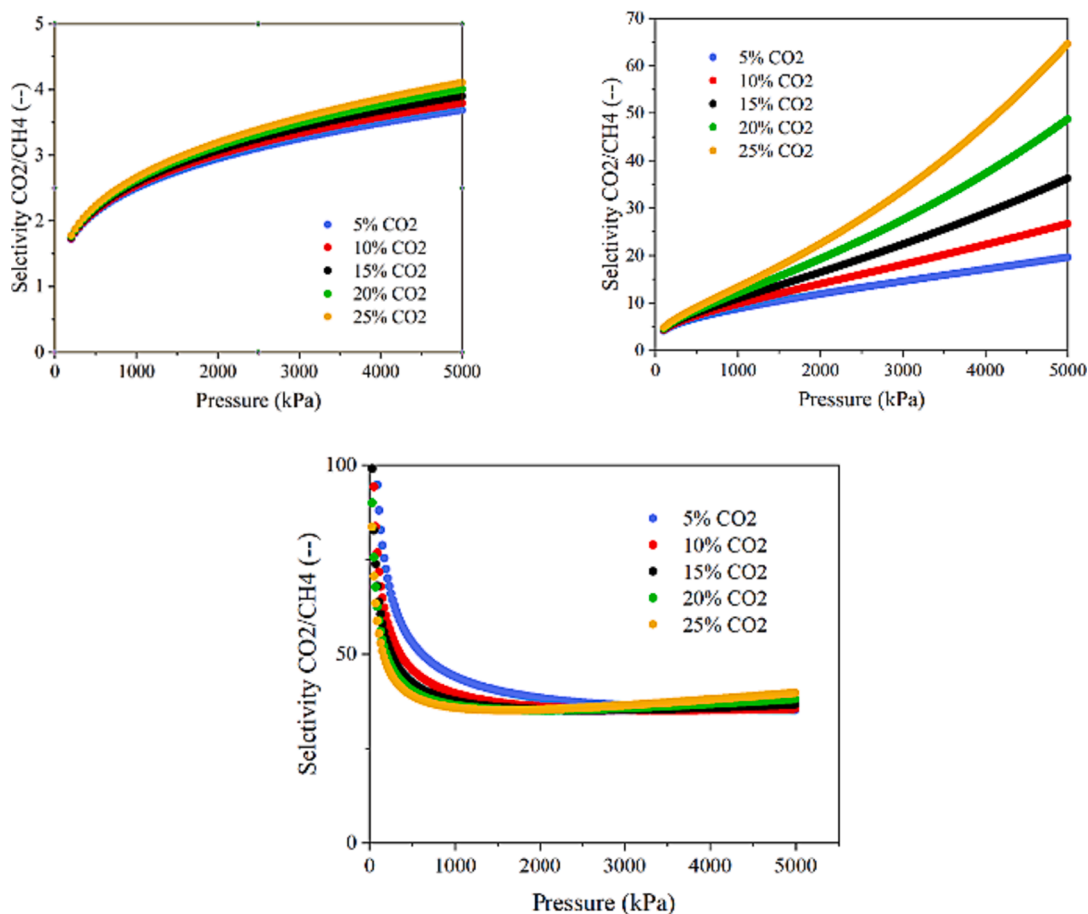

Fig. 8. Represents the co2/ch4 selectivities calculated with the iast theory. the top left graph is the zif-67, the top right graph is the sample zif-67 m1.1 and the bottom graph is the sample ZIF-67 m1.2. The different lines of the graphs represent the selectivity for different CO2 partial pressures.

Declaration of Competing Interest

The authors declare that they have no known competing financial interests or personal relationships that could have appeared to influence the work reported in this paper.

Data availability

No data was used for the research described in the article.

Acknowledgements

Appendix A. Supplementary data

Supplementary data to this article can be found online at https://doi.org/10.1016/j.cej.2023.146846.

References

[1] C. Duan, Y. Yu, H. Hu, Recent progress on synthesis of ZIF-67-based materials and their application to heterogeneous catalysis, Green, Energy Environ. 7 (2022) 3–15.

[2] L. Bastin, P.S. Bárcia, E.J. Hurtado, J.A.C. Silva, A.E. Rodrigues, B. Chen, A Microporous Metal−Organic Framework for Separation of CO2/N2 and CO2/CH4 by Fixed-Bed Adsorption, J. Phys. Chem. C 112 (2008) 1575–1581, https://doi.org/10.1021/jp077618g.

[3] L.A.M. Rocha, K.A. Andreassen, C.A. Grande, Separation of CO2/CH4 using carbon molecular sieve (CMS) at low and high pressure, Chem. Eng. Sci. 164 (2017) 148–157.

[4] J. Duan, M. Higuchi, S. Horike, M.L. Foo, K.P. Rao, Y. Inubushi, T. Fukushima, S. Kitagawa, High CO2/CH4 and C2 Hydrocarbons/CH4 Selectivity in a Chemically Robust Porous Coordination Polymer, Adv. Funct. Mater. 23 (2013) 3525–3530.

[5] V. Safarifard, S. Rodríguez-Hermida, V. Guillerm, I. Imaz, M. Bigdeli, A.A. Tehrani, J. Juanhuix, A. Morsali, M.E. Casco, J. Silvestre-Albero, E.V. Ramos-Fernandez, D. Maspoch, Influence of the Amide Groups in the CO2/N2 Selectivity of a Series of Isoreticular, Interpenetrated Metal-Organic Frameworks, Cryst. Growth Des. 16 (2016) 6016–6023, https://doi.org/10.1021/acs.cgd.6b01054.

[6] W. Wang, D. Yuan, Mesoporous carbon originated from non-permanent porous MOFs for gas storage and CO2/CH4 separation, Sci. Rep. 4 (2014) 5711, https://doi.org/10.1038/srep05711.

[7] N.A.H.M. Nordin, A.F. Ismail, A. Mustafa, R.S. Murali, T. Matsuura, The impact of ZIF-8 particle size and heat treatment on CO2/CH4 separation using asymmetric mixed matrix membrane, RSC Adv. 4 (2014) 52530–52541, https://doi.org/10.1039/C4RA08460H.

[8] E. Alper, O. Yuksel Orhan, CO2 utilization: Developments in conversion processes, Petroleum. 3 (2017) 109–126. https://doi.org/https://doi.org/10.1016/j.petlm.2016.11.003.

[9] C.A. Grande, R.P.P.L. Ribeiro, A.E. Rodrigues, Challenges of electric swing adsorption for CO2 capture, ChemSusChem 3 (2010) 892–898, https://doi.org/10.1002/cssc.201000059.

[10] C. Hepburn, E. Adlen, J. Beddington, E.A. Carter, S. Fuss, N. Mac Dowell, J.C. Minx, P. Smith, C.K. Williams, The technological and economic prospects for CO2 utilization and removal, Nature 575 (2019) 87–97, https://doi.org/10.1038/s41586-019-1681-6.

[11] N. Mac Dowell, P.S. Fennell, N. Shah, G.C. Maitland, The role of CO2 capture and utilization in mitigating climate change, Nature Climate Change 2017 7:4. 7 (2017) 243–249. https://doi.org/10.1038/nclimate3231.

[12] B. Seoane, J. Coronas, I. Gascon, M.E. Benavides, O. Karvan, J. Caro, F. Kapteijn, J. Gascon, Metal–organic framework based mixed matrix membranes: a solution for highly efficient CO2 capture? Chem. Soc. Rev. 44 (2015) 2421–2454, https://doi.org/10.1039/C4CS00437J.

[13] A.C. Pérez-Sequera, M.A. Díaz-Pérez, J.C. Serrano-Ruiz, Recent advances in the electroreduction of CO2 over heteroatom-doped carbon materials, Catalysts 10 (2020) 1–20, https://doi.org/10.3390/catal10101179.

[14] Z. Wan, G. Zhou, Z. Dai, L. Li, N. Hu, X. Chen, Z. Yang, Separation Selectivity of CH4/CO2 Gas Mixtures in the ZIF-8 Membrane Explored by Dynamic Monte Carlo Simulations, Journal of Chemical Information and Modeling 60 (2020) 2208–2218, https://doi.org/10.1021/acs.jcim.0c00114.

[15] B. Zornoza, A. Martinez-Joaristi, P. Serra-Crespo, C. Tellez, J. Coronas, J. Gascon, F. Kapteijn, Functionalized flexible MOFs as fillers in mixed matrix membranes for

[16] highly selective separation of CO2 from CH4 at elevated pressures, Chem. Commun. 47 (2011) 9522–9524, https://doi.org/10.1039/c1cc13431k.

[16] S. Biswas, J. Zhang, Z. Li, Y.-Y. Liu, M. Grzywa, L. Sun, D. Volkmer, P. Van Der Voort, Enhanced selectivity of CO2 over CH4 in sulphonate-, carboxylate- and iodo-functionalized UiO-66 frameworks, Dalton Trans. 42 (2013) 4730–4737, https://doi.org/10.1039/C3DT32288B.

[17] W. Morris, B. Volosskiy, S. Demir, F. Gándara, P.L. McGrier, H. Furukawa, D. Cascio, J.F. Stoddart, O.M. Yaghi, Synthesis, Structure, and Metalation of Two New Highly Porous Zirconium Metal-Organic Frameworks, Inorg. Chem. 51 (2012) 6443–6445, https://doi.org/10.1021/ic300825s.

[18] M. Fakhroleslam, S. Fatemi, Comparative simulation study of PSA, VSA, and TSA processes for purification of methane from CO2 via SAPO-34 core-shell adsorbent, Sep. Sci. Technol. 51 (2016) 2326–2338, https://doi.org/10.1080/01496395.2016.1210640.

[19] I. Stassen, N. Burtch, A. Talin, P. Falcaro, M. Allendorf, R. Ameloot, An updated roadmap for the integration of metal-organic frameworks with electronic devices and chemical sensors, Chem. Soc. Rev. 46 (2017) 3185–3241, https://doi.org/10.1039/c7cs00122c.

[20] D. Mateo, J.L. Cerrillo, S. Durini, J. Gascon, Fundamentals and applications of photo-thermal catalysis, Chem. Soc. Rev. 50 (2021) 2173–2210, https://doi.org/10.1039/D0CS00357C.

[21] S.M.J. Rogge, A. Bavykina, J. Hajek, H. Garcia, A.I. Olivos-Suarez, A. Sepúlveda-Escribano, A. Vimont, G. Clet, P. Bazin, F. Kapteijn, M. Daturi, E.V. Ramos-Fernandez, F.X.I. Llabrés Xamena, V. Van Speybroeck, J. Gascon, Metal-organic and covalent organic frameworks as single-site catalysts, Chem. Soc. Rev. 46 (2017) 3134–3184, https://doi.org/10.1039/c7cs00033b.

[22] Q. Yang, X.u. Qiang, Q. Hai-Long Jiang, Q. Yang, H.-L. Xu, Metal–organic frameworks meet metal nanoparticles: synergistic effect for enhanced catalysis, Chem. Soc. Rev. 46 (2017) 4774–4808, https://doi.org/10.1039/C6CS00724D.

[23] Q.L. Zhu, Q. Xu, Metal-organic framework composites, Chem. Soc. Rev. 43 (2014) 5468–5512, https://doi.org/10.1039/c3cs60472a.

[24] Z. Wang, S.M. Cohen, Postsynthetic modification of metal-organic frameworks, Chem. Soc. Rev. 38 (2009) 1315–1329, https://doi.org/10.1039/b802258p.

[25] M. Ding, R.W. Flaig, H.L. Jiang, O.M. Yaghi, Carbon capture and conversion using metal-organic frameworks and MOF-based materials, Chem. Soc. Rev. 48 (2019) 2783–2828, https://doi.org/10.1039/c8cs00829a.

[26] L. Figueroa-Quintero, D. Villalgordo-Hernández, J.J. Delgado-Marín, J. Narciso, V. K. Velisoju, P. Castaño, J. Gascón, E.V. Ramos-Fernández, Post-Synthetic Surface Modification of Metal-Organic Frameworks and Their Potential Applications, Small Methods. 7 (2023), https://doi.org/10.1002/smtd.202201413.

[27] M. Erkartal, U. Erkilic, B. Tam, H. Usta, O. Yazaydin, J.T. Hupp, O.K. Farha, U. Sen, From 2-methylimidazole to 1,2,3-triazole: a topological transformation of ZIF-8 and ZIF-67 by post-synthetic modification, Chem. Commun. 53 (2017) 2028–2031, https://doi.org/10.1039/C6CC08746A.

[28] R.-B. Lin, D. Chen, Y.-Y. Lin, J.-P. Zhang, X.-M. Chen, A Zeolite-Like Zinc Triazolate Framework with High Gas Adsorption and Separation Performance, Inorg. Chem. 51 (2012) 9950–9955, https://doi.org/10.1021/ic301463z.

[29] G. Zhong, D. Liu, J. Zhang, The application of ZIF-67 and its derivatives: Adsorption, separation, electrochemistry and catalysts, J Mater Chem A Mater. 6 (2018) 1887–1899, https://doi.org/10.1039/c7ta08268a.

[30] J.J. Delgado-Marín, A. Rendón-Patiño, V.K. Velisoju, G.S. Kumar, N. Zambrano, M. Rueping, J. Gascón, P. Castaño, J. Narciso, E.V. Ramos-Fernández, Leaching in Specific Facets of ZIF-67 and ZIF-L Zeolitic Imidazolate Frameworks During the CO2Cycloaddition with Epichlorohydrin, Chem. Mater. (2022), https://doi.org/10.1021/acs.chemmater.2c03374.

[31] M. Costa Gomes, L. Pison, C. Červinka, A. Padua, Porous Ionic Liquids or Liquid Metal-Organic Frameworks? Angewandte Chemie - International Edition. 57 (2018) 11909–11912, https://doi.org/10.1002/anie.201805495.

[32] B. Zhang, J. Zhang, B. Han, Assembling Metal-Organic Frameworks in Ionic Liquids and Supercritical CO2, Chem. Asian J. 11 (2016) 2610–2619, https://doi.org/10.1002/asia.201600323.

[33] S. Liu, S. Liu, X. Hou, T. Xu, J. Tong, J. Zhang, B. Ye, B. Liu, Porous Liquid: A Stable ZIF-8 Colloid in Ionic Liquid with Permanent Porosity, Langmuir 34 (2018) 3654–3660, https://doi.org/10.1021/acs.langmuir.7b04212.

[34] Y. Sun, H. Huang, H. Vardhan, B. Aguila, C. Zhong, J.A. Perman, A.M. Al-Enizi, A. Nafady, S. Ma, Facile Approach to Graft Ionic Liquid into MOF for Improving the Efficiency of CO2 Chemical Fixation, ACS Appl. Mater. Interfaces 10 (2018) 27124–27130, https://doi.org/10.1021/acsami.8b08914.

[35] K. Zhou, B. Mousavi, Z. Luo, S. Phatanasri, S. Chaemchuen, F. Verpoort, Characterization and properties of Zn/Co zeolitic imidazolate frameworks vs. ZIF-8 and ZIF-67, J Mater Chem A Mater. 5 (2017) 952–957, https://doi.org/10.1039/C6TA07860E.

[36] A. Zanon, S. Chaemchuen, B. Mousavi, F. Verpoort, 1 Zn-doped ZIF-67 as catalyst for the CO2 fixation into cyclic carbonates, J. CO2 Util. 20 (2017) 282–291, https://doi.org/10.1016/j.jcou.2017.05.026.

[37] Z. Li, X. Huang, C. Sun, X. Chen, J. Hu, A. Stein, B. Tang, Thin-film electrode based on zeolitic imidazolate frameworks (ZIF-8 and ZIF-67) with ultra-stable performance as a lithium-ion battery anode, J. Mater. Sci. 52 (2017) 3979–3991, https://doi.org/10.1007/s10853-016-0660-7.

[38] P. Krokidas, M. Castier, S. Moncho, D.N. Sredojevic, E.N. Brothers, H.T. Kwon, H.-K. Jeong, J.S. Lee, I.G. Economou, ZIF-67 Framework: A Promising New Candidate for Propylene/Propane Separation, Experimental Data and Molecular Simulations, the Journal of Physical Chemistry c. 120 (2016) 8116–8124, https://doi.org/10.1021/acs.jpcc.6b00305.

[39] M. Savonnet, S. Aguado, U. Ravon, D. Bazer-Bachi, V. Lecocq, N. Bats, C. Pinel, D. Farrusseng, Solvent free base catalysis and transesterification over basic

functionalised Metal-Organic Frameworks, Green Chem. 11 (2009) 1729–1732, https://doi.org/10.1039/B915291C.

[40] M.E. Casco, Y.Q. Cheng, L.L. Daemen, D. Fairen-Jimenez, E.V. Ramos-Fernández, A.J. Ramirez-Cuesta, J. Silvestre-Albero, Gate-opening effect in ZIF-8: The first experimental proof using inelastic neutron scattering, Chem. Commun. 52 (2016) 3639–3642, https://doi.org/10.1039/c5cc10222g.

[41] M.E. Casco, J. Fernández-Catalá, Y. Cheng, L. Daemen, A.J. Ramirez-Cuesta, C. Cuadrado-Collados, J. Silvestre-Albero, E.V. Ramos-Fernandez, Understanding ZIF-8 Performance upon Gas Adsorption by Means of Inelastic Neutron Scattering, ChemistrySelect 2 (2017) 2750–2753, https://doi.org/10.1002/slct.201700250.

[42] X. Qu, G. Pan, L. Zheng, S. Chen, Y. Zhou, S. Zhang, 3D Cobalt(II)-based MOF: Synthesis, structure, thermal decomposition behavior and magnetic property, J. Solid State Chem. 305 (2022) 122702.

[43] F. Billes, I. Ziegler, H. Mikosch, Vibrational spectroscopic study of sodium-1,2,4-triazole, an important intermediate compound in the synthesis of several active substances, Spectrochim. Acta A Mol. Biomol. Spectrosc. 153 (2016) 349–362.

[44] M. Pagacz-Kostrzewa, J. Krupa, W. Gul, M. Wierzejewska, FTIR matrix isolation studies of thermal decomposition of 1,2,4-triazolyl-3-carboxylic acid, J. Mol. Struct. 1209 (2020), 127938.

[45] K. Mucha, M. Pagacz-Kostrzewa, J. Krupa, M. Wierzejewska, Structure and IR spectroscopic properties of complexes of 1,2,4-triazole and 3-amino-1,2,4-triazole with dinitrogen isolated in solid argon, Spectrochim. Acta A Mol. Biomol. Spectrosc. 285 (2023), 121901.

[46] S. Mukherjee, M. Das, A. Manna, R. Krishna, S. Das, Newly designed 1,2,3-triazole functionalized covalent triazine frameworks with exceptionally high uptake capacity for both CO2 and H2, J Mater Chem A Mater. 7 (2019) 1055–1068, https://doi.org/10.1039/C8TA08185A.

[47] X. Wu, W. Liu, H. Wu, X. Zong, L. Yang, Y. Wu, Y. Ren, C. Shi, S. Wang, Z. Jiang, Nanoporous ZIF-67 embedded polymers of intrinsic microporosity membranes with enhanced gas separation performance, J Memb Sci. 548 (2018) 309–318, https://doi.org/10.1016/j.memsci.2017.11.038.

[48] D.G. Brown, U. Weser, XPS Spectra of Spin-Triplet Cobalt(III), Complexes 34 (1979) 1468–1470.

[49] M. Ronda-Lloret, I. Pellicer-Carreño, A. Grau-Atienza, R. Boada, S. Diaz-Moreno, J. Narciso-Romero, J.C. Serrano-Ruiz, A. Sepúlveda-Escribano, E.V. Ramos-Fernandez, Mixed-Valence Ce/Zr Metal-Organic Frameworks: Controlling the Oxidation State of Cerium in One-Pot Synthesis Approach, Adv. Funct. Mater. 31 (2021), https://doi.org/10.1002/adfm.202102582.

[50] R. Krishna, J.M. van Baten, How Reliable Is the Ideal Adsorbed Solution Theory for the Estimation of Mixture Separation Selectivities in Microporous Crystalline Adsorbents? ACS Omega 6 (2021) 15499–15513, https://doi.org/10.1021/acsomega.1c02136.

[51] Y. Jiang, J. Hu, L. Wang, W. Sun, N. Xu, R. Krishna, S. Duttwyler, X. Cui, H. Xing, Y. Zhang, Comprehensive Pore Tuning in an Ultrastable Fluorinated Anion Cross-Linked Cage-Like MOF for Simultaneous Benchmark Propyne Recovery and Propylene Purification, Angew. Chem. Int. Ed. 61 (2022) e202200947.

[52] F.R. Siperstein, C. Avendaño, J.J. Ortiz, A. Gil-Villegas, Analytic expressions for the isosteric heat of adsorption from adsorption isotherm models and two-dimensional SAFT-VR equation of state, AIChE J 67 (2021) e17186.

[53] N. Tzabar, H.J.M. ter Brake, Adsorption isotherms and Sips models of nitrogen, methane, ethane, and propane on commercial activated carbons and polyvinylidene chloride, Adsorption 22 (2016) 901–914, https://doi.org/10.1007/s10450-016-9794-9.